Using MR Techniques to Probe Permeability Reduction in Rock Cores

M. L. Johns, A. J. Sederman and L. F. Gladden
Dept. of Chemical Engineering, University of Cambridge, Cambridge, CB2 3RA, UK

A. Wilson and S. Davies
Schlumberger Cambridge Research, Cambridge, CB3 0EL, UK

Polymer solutions are used commonly in oil-recovery applications to reduce water production. While the polymer treatment is known to modify the permeability of the rock, the mechanism by which this occurs is poorly understood, and, hence, the ability to optimize either the polymer solution or its application is restricted. In this work, the pulsed-gradient spin-echo nuclear magnetic resonance technique is used to determine displacement propagators (distributions) for brine solution flowing through a Bentheimer sandstone rock core, both before and after treatment of the rock core with a polyacrylamide polymer solution. A novel simulation strategy employing the lattice–Boltzmann method is then proposed to interpret the differences in these propagators in terms of the location of polymer retained within the pore structure of the rock following treatment. The results suggest that the polymer is preferentially trapped in comparatively low permeability pores.

Introduction

Recovery of water, as well as the desired oil, during an oil-recovery process gives rise to significant costs related to both the treatment and subsequent disposal of the contaminated water (Akhnoukh et al., 1999). In an attempt to reduce this problem, a polymer treatment is often introduced into the water-containing regions of the reservoir. The polymer is intended to reduce the permeability of the rock and, hence, also the production of water at the oil well. However, the exact mechanism whereby the polymer reduces the permeability of the rock is generally not well understood, which restricts our ability to optimize both the polymer formulation and its application.

The motivation for this study was to explore the modification of the pore space by the polymer using a combination of magnetic resonance measurements (pulsed-gradient-spin echo nuclear magnetic resonance (PGSE NMR) techniques) of brine transport within the pore structure of the rock, both before and after polymer treatment, and a subsequent numerical simulation study of the differences in the resultant experimental data. With respect to the simulations performed, two limiting cases were considered with respect to the location of the retained polymer: (i) the polymer adsorbed uniformly throughout the pore space, and (ii) certain pores are preferentially blocked with polymer, thereby modifying the connectivity of the pore space (polymer adsorption followed by polymer entanglement and retention in pores characterized by comparatively low shears). This combination of experimental and simulation techniques enables the effect of the polymer treatment to be both investigated noninvasively and interpreted at a pore scale.

PGSE NMR techniques, which are designed to provide displacement propagator measurements, are well established as an experimental technique for probing molecular transport in porous media. Displacement propagators, $P(\boldsymbol{R},\Delta)$, are molecular probability distributions of displacement, $\boldsymbol{R}$, in a particular direction over a time period, Δ. A large body of literature exists in which PGSE NMR displacement propagators of flow through a porous medium have been acquired (for example, Packer and Tessier, 1996; Lebon et al., 1996; Amin et al., 1997; Seymour and Callaghan, 1997; Van As and Dusschoten, 1997; Tessier and Packer, 1998; Stapf et al., 1998;

Correspondence concerning this article should be addressed to M. L. Johns.

Manz et al., 1999a). Propagators can be considered as a type of tracer experiment. Their main advantage over conventional tracer experiments is that they do not require the introduction of an exogenous tracer material into the flowing stream, as the fluid itself can provide the necessary NMR signal. In addition, by simply varying the observation time, Δ, over which the displacement of the molecules is observed, the displacement propagators are able to probe motion at different length scales. In porous media, at short values of Δ, the propagator is determined by flow and diffusion within single pores. As Δ is increased, the propagator will reflect motion between pores.

In this study, significant differences were observed between displacement propagators (recorded using the same value of Δ) when measured before and after the rock was exposed to a polymer treatment. To interpret these differences, a numerical simulation of fluid transport within a 3-D porous lattice was performed. The simulation lattice was constructed such that it was characterized by the same porosity and surface-to-volume ratio as the actual experimental rock used. The flow field in the lattice was determined using the lattice–Boltzmann simulation technique (for example, Manz et al., 1999b) and displacement propagators generated from the resulting flow fields. Good agreement was found between the experimentally determined and predicted propagators for the system prior to polymer treatment. By modifying the simulation lattice and repeating the numerical simulation, it was possible to identify potential preferred polymer locations within the pore structure by comparing the predicted propagators to those measured experimentally using the actual rock sample after exposure to the polymer treatment.

Experimental Methodology

Materials used

The cylindrical rock core used was composed of Bentheimer sandstone with a diameter of 38.4 mm, a length of 70 mm, and a porosity, σ, of 21% (determined gravimetrically). The polymer solution is commercially available and consists of a partially hydrolyzed polyacrylamide with an average molecular weight of approximately 2.5 million. The brine solution consisted of 2 wt % KCL in water, and was filtered and degassed. The polymer treatment consisted of 5 g/L of the polymer in brine solution. Both the rock core and the treatment fluid were supplied by Schlumberger Cambridge Research. The rock core was contained in the flow cell, shown in Figure 1, during the course of the experiments. In the flow cell, the rock core is placed in a rubber sleeve. The outside surface of the sleeve is pressurized by a fluorocarbon, Fluorinet 40, which was obtained form Aldrich, UK. Hence, the brine solution is forced to flow through the rock core. This containing fluid provides no NMR signal, as only ^{1}H nuclei in a liquid are detected in the NMR experiments performed.

NMR methods used

All displacement propagators were produced with a Bruker Spectrospin DMX 200 NMR spectrometer equipped with a 4.77 T 15-cm vertical bore magnet and shielded magnetic gradients providing a maximum gradient strength of 19 G/cm.

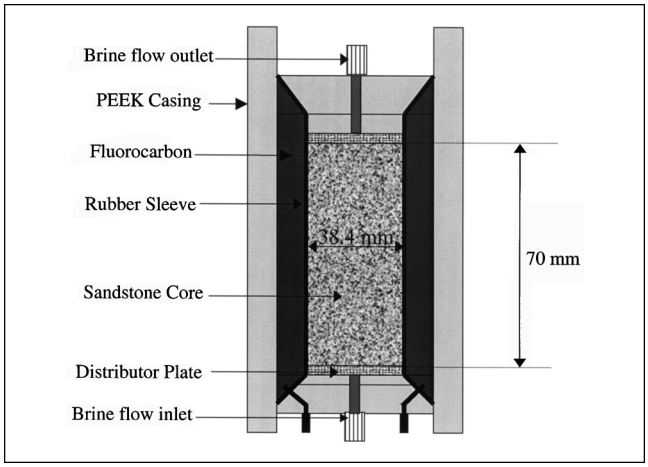

Figure 1. Cross-sectional view of the flow cell used.

The sandstone rock core is contained in a rubber sleeve, which is pressurized from the outside using a fluorocarbon, Fluorinet 40. This thus delivers no NMR signal, as only ^{1}H nuclei are detected. The sleeve forces the brine solution to flow through the cylindrical rock core is an axial direction.

We used a bird-cage radio-frequency coil with a diameter of 63 mm and tuned to 199.98 MHz for the ^{1}H resonance.

The measurement of propagators is conventionally performed using the pulsed-gradient stimulated-echo (PGSTE) pulse sequence shown in Figure 2a. A matching pair of mag-

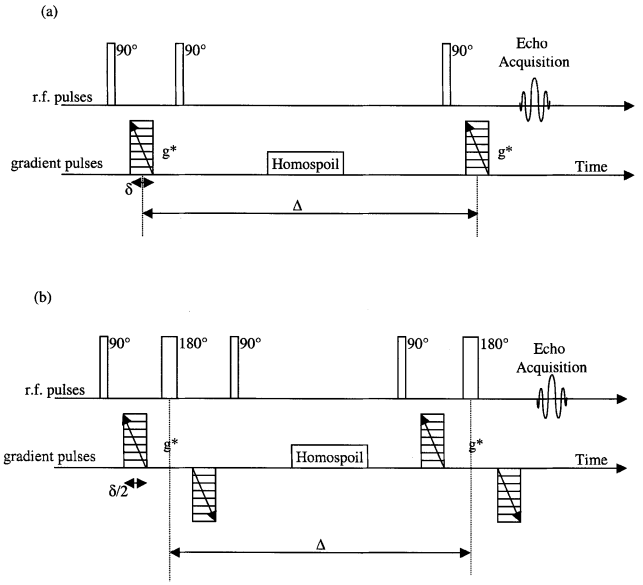

Figure 2. Pulsed-gradient stimulated-echo pulse sequences used to produce the propagators.

The strength of the g^* gradient pulses is ramped up in set increments. The propagator, $P(\boldsymbol{R},\Delta)$, is extracted from the resulting data, $\boldsymbol{E}(\boldsymbol{q},\Delta)$, using Eq. 2. In the rock cores, magnetic susceptibility gradients can distort the acquired propagator. These are minimized using the alternating pulsed-field-gradient stimulated-echo (APGSTE) pulse sequence (Cotts et al., 1989), shown in Figure 2b. The 180° rf pulses refocus the phase shift in the acquired signal due to these magnetic susceptibility gradients.

netic-field gradients (g^*) of strength $\boldsymbol{g}$, duration δ, and temporal separation Δ, are applied along with a sequence of 90° rf pulses. The first gradient imparts a phase shift $\phi(\boldsymbol{r}) = \gamma\delta\boldsymbol{g}\cdot\boldsymbol{r}$ to the ^{1}H nuclei at position $\boldsymbol{r}$. This phase shift is then inverted by the following two 90° rf pulses. If the ^{1}H nuclei have moved to position $\boldsymbol{r}'$ during the time period Δ, the net phase shift of the ^{1}H nuclei is $\phi(\boldsymbol{r}\text{-}\boldsymbol{r}') = \gamma\delta\boldsymbol{g}\cdot(\boldsymbol{r}-\boldsymbol{r}')$. When the ^{1}H nuclei are experiencing Brownian motion, a Gaussian distribution of phase shifts results if the ^{1}H nuclei diffuse in an unrestricted environment. The resultant attenuation of the NMR signal is given by the following formula (Callaghan, 1991)

$$\boldsymbol{E}(\boldsymbol{q},\Delta) = \exp\left[-D\boldsymbol{q}^2(\Delta - \delta/3)\right] \tag{1}$$

where $\boldsymbol{q} = (1/2\pi)\gamma\delta\boldsymbol{g}$, D is the self-diffusion coefficient and $\boldsymbol{E}(\boldsymbol{q},\Delta)$ is the echo intensity normalized by the value when $\boldsymbol{q}$ equals 0. Thus, by measuring $\boldsymbol{E}(\boldsymbol{q},\Delta)$ as a function of $\boldsymbol{q}$, we are able to determine the value of D. In the case of restricted diffusion, as in the rock samples studied in this work, Eq. 1 is still a good approximation of the value of D as $\boldsymbol{q}$ tends to 0 (Latour et al., 1993).

The distribution of the phase shifts of the ^{1}H nuclei will reflect the distribution of their displacements ($\boldsymbol{r}\text{-}\boldsymbol{r}'$) over the observation time, Δ. This distribution of phase shifts, and, hence, the distributions of displacement, can be accessed using the following procedure. Defining a dynamic displacement, $\boldsymbol{R} = (\boldsymbol{r}\text{-}\boldsymbol{r}')$, the displacement propagator, $\boldsymbol{P}(\boldsymbol{R},\Delta)$, is the probability distribution of $\boldsymbol{R}$ for the ^{1}H nuclei over the time period, Δ. $\boldsymbol{P}(\boldsymbol{R},\Delta)$ can be related to $\boldsymbol{E}(\boldsymbol{q},\Delta)$ by the following relationship (Callaghan, 1991)

$$\boldsymbol{E}(\boldsymbol{q},\Delta) = \int \boldsymbol{P}(\boldsymbol{R},\Delta)\exp(i2\pi\boldsymbol{q}\cdot\boldsymbol{R})\,d\boldsymbol{R} \tag{2}$$

Thus, $\boldsymbol{P}(\boldsymbol{R},\Delta)$ is the Fourier transform of $\boldsymbol{E}(\boldsymbol{q},\Delta)$, and, hence, by measuring $\boldsymbol{E}(\boldsymbol{q},\Delta)$ as a function of $\boldsymbol{q}$ and Fourier transforming the resultant data with respect to $\boldsymbol{q}$, we can produce the displacement propagator, $\boldsymbol{P}(\boldsymbol{R},\Delta)$.

In typical rock samples, susceptibility differences between the solid and liquid phases result in internal magnetic gradients at the liquid–solid interfaces. These can severely distort the displacement propagators as they dephase, and, hence, attenuate the signal in the same manner as the applied magnetic gradients, g^*. Fortunately, in Bentheimer sandstone, the low concentration of paramagnetic species results in these susceptibility differences being comparably small. In addition, the effect of the internal magnetic gradients was further reduced by using the alternating pulsed-gradient stimulated-echo (APGSTE) pulse sequence shown in Figure 2b, which was developed by Cotts et al. (1989). The two 180° rf pulses refocus the dephasing effects of the internal magnetic gradients, but not the two applied magnetic gradients of the opposite direction on either side of each 180° rf pulse.

Experiments performed

The rock cores were vacuum-saturated with brine solution and placed in the flow cell shown in Figure 1. The diffusion coefficient of the brine solution in the rock core was determined at the following values of Δ: 40 ms, 60 ms, 90 ms, 120 ms, 180 ms, 250 ms, and 500 ms. Brine solution was then pumped through the rock core and displacement propagators acquired in an axial, and, hence, superficial flow direction. This was done at the following observation times: 100 ms, 200 ms, 500 ms, and 1,000 ms, and at the following flow rates of brine solution: 5 mL/min and 10 mL/min. Each combination of flow rate and observation time was repeated twice to check for reproducibility. The polymer treatment fluid was then pumped through the rock core at a flow rate of 1 mL/min over a period of 2 h. Brine solution was then pumped back into the cell, in the process displacing most of the contained polymer treatment fluid. Approximately 4% of the pore volume was occupied by retained polymer solution; this value was estimated by measuring the amount and concentration of the polymer solution displaced from the rock core by the brine solution. Once the pressure drop across the sample had stabilized (that is, no more treatment fluid was being removed from the rock core), the acquisition of the propagators was repeated at the same observation times and flow rates of brine solution as described previously.

Modeling Approach

Ideally, in order to simulate the displacement propagators, a 3-D image of the pore space in the rock core would be desirable. This is unfortunately not possible at a reasonable resolution using MRI in the presence of magnetic susceptibility gradients, such as those found in the rock core. Hence, a model lattice of the pore space was generated using the following procedure.

Generation of model pore-space lattice

A 3-D image of the pore space of a water-saturated random packing of a 5-mm-dia. glass ballotini was acquired using MRI. The packing was contained in a cylindrical glass container of diameter 46.6 mm. The image consisted of a matrix of $128\times128\times128$ voxels (volume elements) with an isotropic resolution of 390 μm. Further details concerning the acquisition of the image are contained in Sederman et al. (1997). Morphological thinning (Baldwin et al., 1996) was then applied to this model lattice until a porosity of 21% was produced. This value matches the porosity of the actual rock core used. In morphological thinning, voxels in the pore space that are adjacent to voxels containing solid, are stripped away and allocated to be solid. Voxels with the highest number of faces in contact with the solid material are stripped away first. This procedure was repeated until the porosity of the image equalled the desired amount (21%). A similar approach was adopted by Roberts and Schwartz (1989), and is believed to mimic the diagnestic process whereby sandstone is formed from an unconsolidated packing of sand particles.

Alternative techniques are available to generate the model pore-space lattice, in particular the use of various reconstruction algorithms to generate an image of a porous medium. A far more satisfactory approach, however, would to be image it directly. Current work is focusing on applying X-ray microtomography to this use.

A length scale was also required for the model lattice so that the characteristic average pore dimension in the model lattice approximated that in the actual rock core. To achieve

this the following procedure was adopted: Mitra et al. (1993) and Hurlimann et al. (1994) showed that the surface-to-volume ratio (s/v) of various rock samples could be estimated by measuring the diffusion coefficient, D, of the contained fluid using NMR PFG techniques, as a function of observation time, Δ. The relationship between D and Δ, at small values of Δ, is (Mitra et al., 1993)

$$\frac{D}{D_0} = 1 - \frac{s}{\nu}\frac{4}{9\pi^{0.5}}(D_0\Delta)^{0.5} \tag{3}$$

where D_0 is the unrestricted diffusion-coefficient of the contained fluid. Hence, the diffusion coefficient of the brine solution in the rock core was measured as a function of Δ, using Eq. 2. These data were used to determine the s/v ratio of the rock core, using Eq. 3. The length scale of the lattice model was then adjusted to match this value. Thus, the lattice model had both a porosity and a surface-to-volume ratio that were equal to those of the rock core used.

Generation of displacement propagators

In order to produce the displacement propagators for the model pore space, a description of the 3-D velocity field in the pore space is first required. This was generated using a lattice–Boltzmann simulation. The average pore-scale velocity, v_p, for the rock core could be calculated using the following formula

$$\boldsymbol{\nu}_p = \frac{\boldsymbol{F}}{\boldsymbol{A}\boldsymbol{\sigma}} \tag{4}$$

where $\boldsymbol{F}$ is the imposed volumetric flow rate, $\boldsymbol{A}$ is the cross-sectional area of the rock core, and $\boldsymbol{\sigma}$ is the porosity. The values of $\boldsymbol{\nu}_p$ in the lattice–Boltzmann simulations were set equal to the respective experimental values. A comprehensive description of the lattice–Boltzmann technique is contained in Rothman and Zalenski (1998). Its value in the current context is that it is able to efficiently deal with the multiple boundaries encountered in a porous media. It relies on the formation of a rigid lattice in the pore space of the image. Particles are then able to migrate along the bonds in this lattice, and collision rules are implemented that replicate the Navier–Stokes equation. Further details concerning the implementation of this algorithm can be found in Manz et al. (1999b). In Manz et al. (1999b), the lattice–Boltzmann method was verified by direct comparison of the simulated flow field in an image of a random packing of glass ballotini with three-dimensional NMR velocity images of the exact same random packing. Excellent agreement was found between the lattice–Boltzmann simulation results and the experimental velocity images.

With a description of the 3-D velocity field in the model pore space, the propagators were generated in the following manner. A large number of particles (typically 20,000) were released in the model lattice at random positions. Their subsequent motion was determined by the velocity field in jumps lasting 0.1 ms over a total time period, Δ. Diffusion was added by allowing random jumps with a Gaussian probability, satisfying Einstein's equation

$$\mathrm{RMS}^2 = 6D(0.1\,\mathrm{ms}) \tag{5}$$

where RMS^2 is the root-mean-squared displacement due to diffusion. By generating a histogram of the displacement, $\boldsymbol{R}$, of the individual particles over the time period, Δ, the corresponding propagator was determined.

Two scenarios for the adsorption and entrapment of the polymer in the pore space were then considered during the simulations [hereafter referred to as scenario (i) and scenario (ii)].

Scenario (i). The polymer was adsorbed evenly on the surface of the solid material at the edge of the pore space. This was achieved by continuing the morphological thinning procedure until the porosity of the system was reduced from 21% to 17% (as estimated from experimental measurements). All model lattice voxels, which were removed during this thinning stage, were allocated to contain polymer.

Scenario (ii). The pore-space image was segregated into individual pores using the pore-thinning algorithm described in Baldwin et al. (1996). In this algorithm boundaries between pores are defined as local minima in the hydraulic radius of the pore space. The average velocity was then calculated for each pore, using the velocity field provided by the lattice–Boltzmann simulation. The pores with the lowest average velocity were assigned to contain polymer until the porosity of the system (excluding polymer-containing regions) equaled 17%.

For the simulations with polymer present, the velocity field was recalculated using the lattice–Boltzmann method. This was done only for the portion of the pore space containing brine solution; the voxels that contained polymer were treated as solid during simulation of the velocity field. However, in producing the propagators, the particles were allowed to dif-

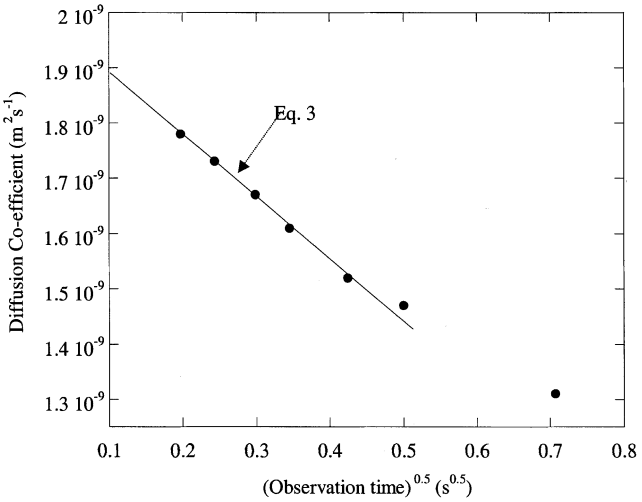

Figure 3. Diffusion coefficient of the brine solution in the rock core as a function of $\Delta^{0.5}$, before the introduction of the polymer treatment.

The surface-to-volume ratio of the pore space was calculated using these data and Eq. 3. The value of s/v for the rock core was calculated to be 52 mm^{-1}.

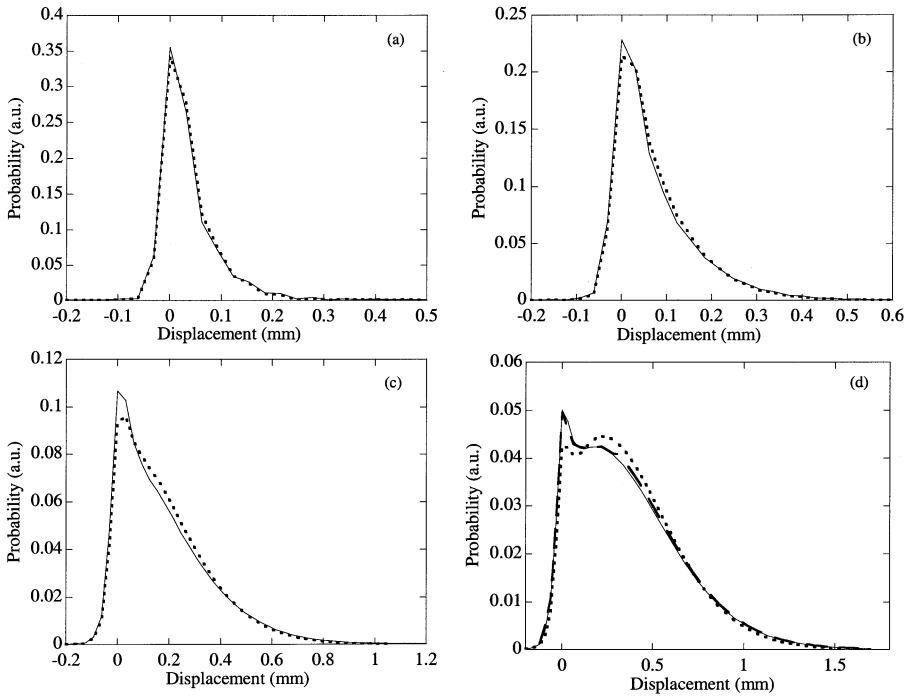

Figure 4. Displacement propagators acquired at a flow rate of 5 mL/min.

The short dashed lines refer to the propagators acquired before polymer treatment, while the solid lines refer to the propagators acquired after polymer treatment. The observation times are (a) 100 ms, (b) 200 ms, (c) 500 ms, and (d) 1,000 ms. The long dashed lines refer to the propagator acquisition repeat performed after treatment. Reproducibility of the propagators is clearly excellent.

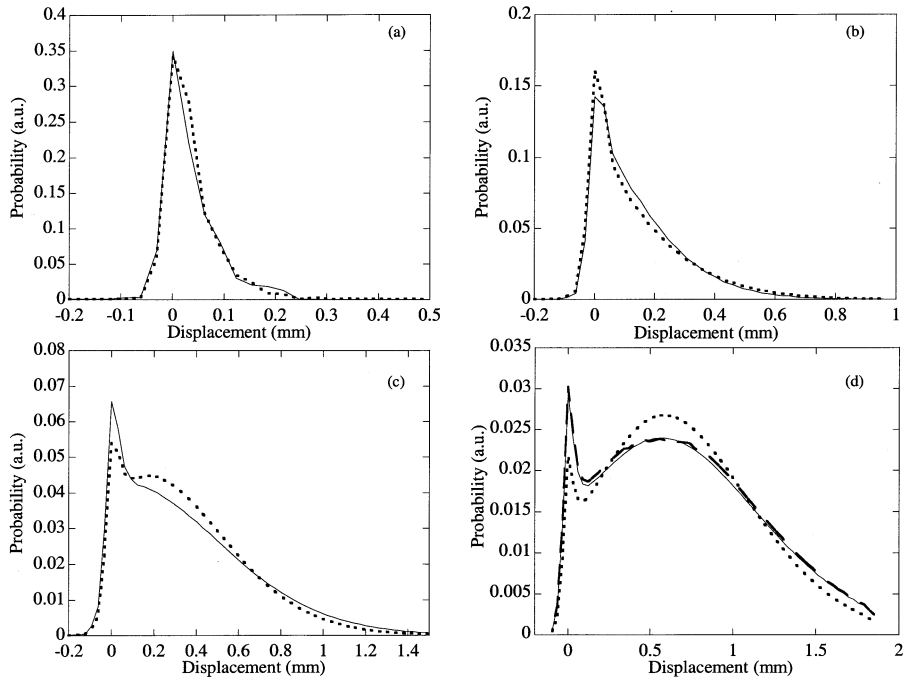

Figure 5. Displacement propagators acquired at a flow rate of 10 mL/min.

The dashed lines refer to the propagators acquired before polymer treatment, while the solid lines refer to the propagators acquired after polymer treatment. The observation times are (a) 100 ms, (b) 200 ms, (c) 500 ms, and (d) 1,000 ms. The long dashed lines refer to the propagator acquisition repeat performed after treatment. Reproducibility of the propagators is clearly excellent.

fuse into the regions occupied by the polymer, where the velocity vector was set equal to zero. Diffusion of water into the polymer regions will occur in the actual rock core, as the polymer treatment fluid is approximately 95 w/w % water. This was confirmed by measuring the diffusion coefficient of the water in the polymer treatment fluid both prior to its use as well as when the treatment fluid was present in the rock core.

Results and Discussion

s/v ratio calculation

In Figure 3, the diffusion coefficient of the brine solution in the rock core is presented as a function of $\Delta^{0.5}$. This data was acquired using the pulse sequence shown in Figure 2b as q tended to zero. Applying Eq. 3 to the data in Figure 3, the s/v ratio of the pore space in the rock core was calculated to be 52 mm^{-1}. The fit of Eq. 3 to the data in Figure 3 is shown by the solid line. Equation 3 is only valid at short values of Δ (Latour et al., 1993); hence, the last two data points in Figure 3 were not included in the fit.

Experimental propagators

The results for the experimental displacement propagators acquired at a flow rate of 5 mL/min are contained in Figure 4, while the displacement propagators for a flow rate of 10 mL/min are contained in Figure 5. The observation times, Δ, in both figures are: (a) 100 ms, (b) 200 ms, (c) 500 ms, and (d) 1,000 ms, respectively. In each figure, the dashed line refers to the propagator acquired before the polymer treatment, while the solid line refers to the propagator acquired after polymer treatment. Reproducibility of these propagators was excellent. As revealed by the repeats shown in Figures 4d and 5d, this was consistently the case for all measurements made. As the value of Δ is increased in both Figures 4 and 5, the shape of the propagator is seen to change from an exponential shape to a Gaussian shape that is centered on the average displacement. This is consistent with previous observations (for example, Lebon et al., 1996), as the length scale probed by the individual ^1H nuclei changes from being predominately within a single pore to motion between pores. As a check on the accuracy of the propagators, the average displacement, d, was calculated separately for each experimental propagator. The actual value of d was determined using Eq. 4 to calculate v_p, and then multiplying v_p by the respective value of Δ. When the values of d, calculated from the propagators, were compared with the actual values, the discrepancy was always less than 6%.

In Figures 4 and 5 at short observation times, Δ, there is no significant difference between the propagators acquired before and after the polymer treatment. However as observation time, Δ, is increased, the posttreatment propagators consistently show a delayed transition from an exponential shape to a Gaussian shape, when compared with the pretreatment propagators. Hence, in the posttreatment propagators, more of the brine solution is essentially stagnant (that is, centered around zero displacement) at large values of Δ. These differences are well in excess of any that could arise due to reproducibility issues. This delayed transition in the posttreatment propagators relative to the pretreatment propagators, is compensated for by an increase in the amount of brine solution that experiences larger displacements. The pressure drop experienced by the brine solution as it flowed through the rock core at a flow rate of 10 mL/min was 0.21 bar. After polymer treatment, the corresponding pressure drop across the rock core for the brine solution at a flow rate of 10 mL/min (after the flow had stabilized) was 0.26 bar.

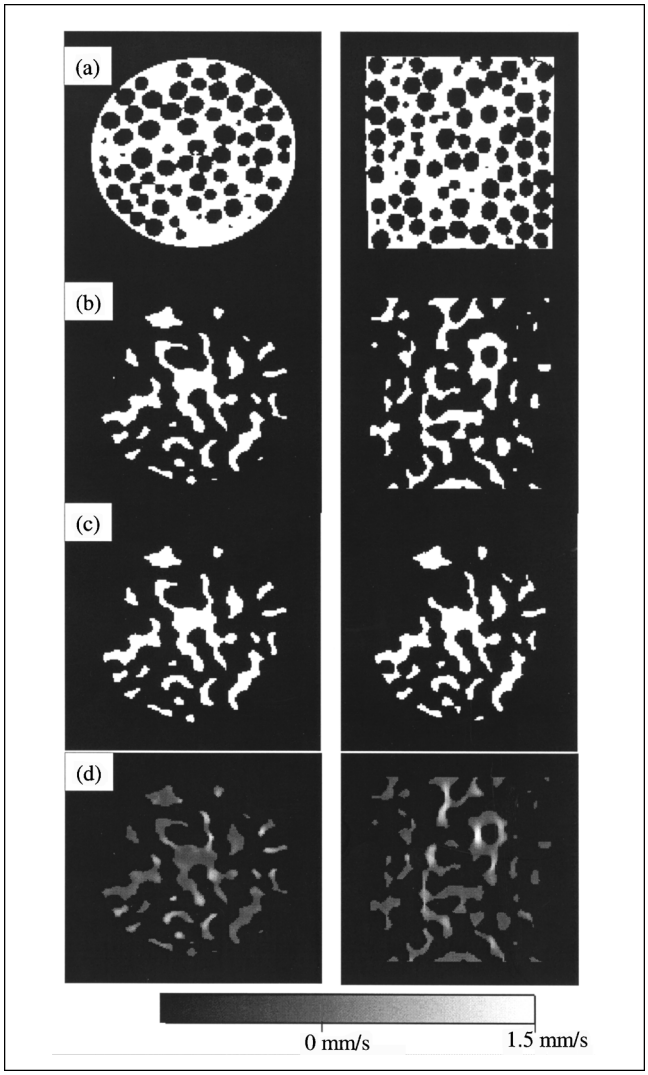

Figure 6. Various stages of the generation of the model pore space.

In Figure 6a, a horizontal and vertical slice is shown from the original 3-D image of the water-saturated packing of glass ballotini. This image was then subjected to morphological thinning until a porosity of 21% was produced, matching that of the actual rock core. The slices corresponding to Figure 6a, are shown in Figure 6b following this thinning procedure. The length scale in the thinned image was then adjusted until the s/v ratio of the pore space equaled 52 mm^{-1}, the value calculated for the actual rock core. The horizontal slice shown in Figure 6b is reproduced in Figure 6c, with areas occupied by polymer being eliminated, for scenarios i and ii, respectively. The velocity field in these structures was then calculated using a lattice–Boltzmann simulation. The axial component of this velocity field, which corresponds to the superficial flow direction, is shown in Figure 6d for the original lattice and the same slices as are shown in Figures 6a and 6b.

This means that the permeability of the rock core, as defined by Darcy's law, was reduced by only 25%. Hence, this highlights the sensitivity of the propagator technique to modest changes in permeability.

The following argument is presented for the fact that the corresponding pre- and posttreatment propagators are similar at short observation times, but differ significantly as the observation time is increased. The water molecules that are virtually stagnant in the posttreatment propagators when compared to the pretreatment propagators at long observation times must have been reasonably stagnant at short observation times in both the pre- and posttreatment propagators. If this were not the case then there would be differences in the pre- and posttreatment propagators at short observation times. As observation time is increased, these "stagnant" molecules have a greater ability in the pretreatment propagator to migrate to different pores that potentially contain higher velocities. Consequently, we hypothesize that the polymer solution was retained in pores characterized by low permeabilities, and, hence, average velocities and shear rates. The retained polymer thus effectively "shut off" the comparatively small amount of flow through these pores. This hypothesis agrees with the observations of Al-Sharji et al. (2001), who measured polyacrylamide polymer retention in 2-D transparent micromodels after displacement by water. They observed that the polymer was retained in relatively stagnant pore space. Our hypothesis will, however, be tested by the simulation results described in the next section.

Simulation results

The various stages of the generation of the model pore space are shown in Figure 6. In Figure 6a, a horizontal and a vertical slice are shown extracted from the original 3-D image of the glass ballotini. Pore space is shown in white and solid material in black. Following the morphological thinning process, the same slices are shown in Figure 6b. As mentioned previously the porosity of this structure (21%) equals that of the original rock core. The length scale in this model pore space was then adjusted so that the s/v ratio equalled 52 mm^{-1}, the value calculated experimentally for the rock core. The modified pore space relevant to polymer retention in scenario (i) and scenario (ii) is shown in Figure 6c. The lattice-Boltzmann code was then used to simulate the 3-D velocity field in these model lattices. The component of this velocity field in the superficial flow direction is shown in Figure 6d for the pretreatment simulation, and the same slices as are shown in Figures 6a and 6b.

The results of the propagator simulations are contained in Figures 7a, 7b, and 7c. In Figure 7a, the solid lines show the

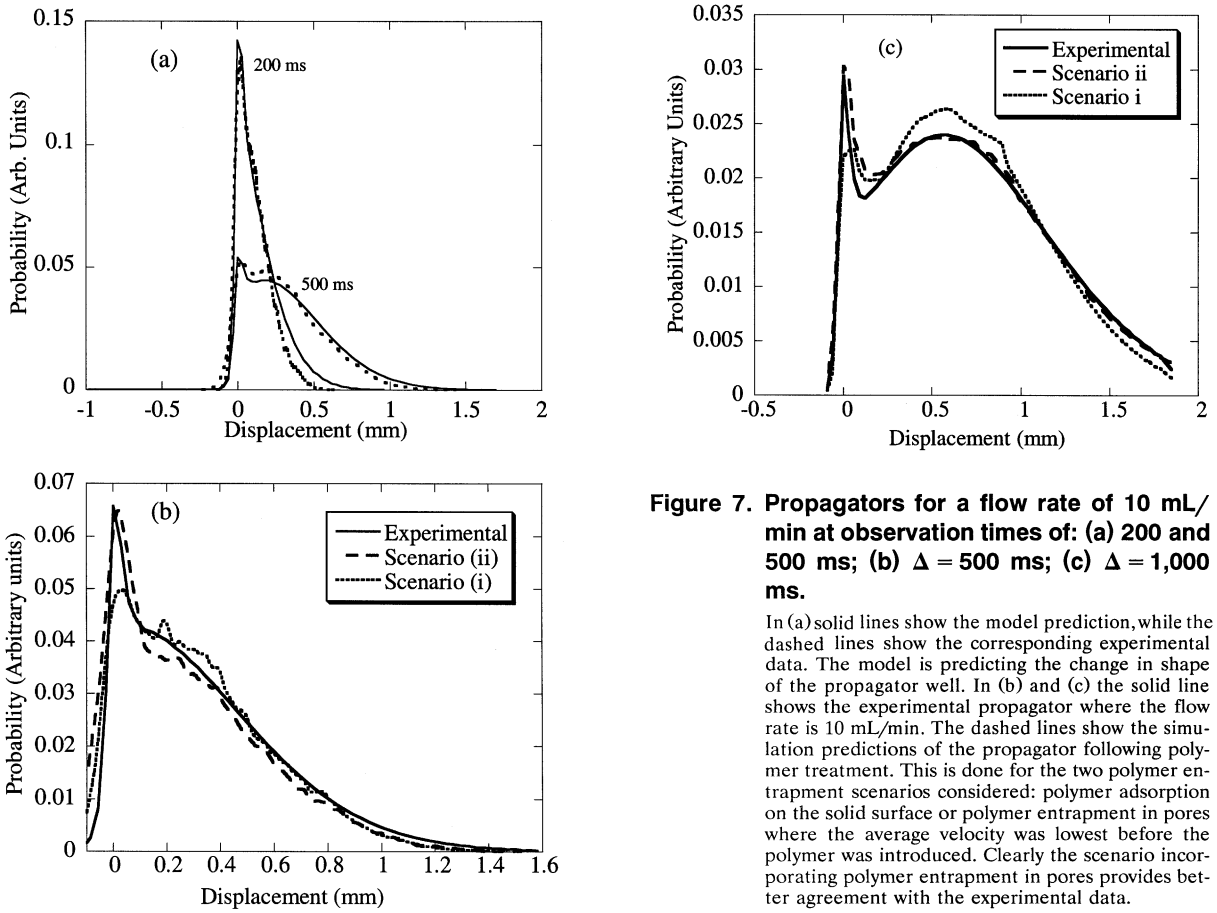

Figure 7. Propagators for a flow rate of 10 mL/min at observation times of: (a) 200 and 500 ms; (b) $\Delta = 500$ ms; (c) $\Delta = 1{,}000$ ms.

In (a) solid lines show the model prediction, while the dashed lines show the corresponding experimental data. The model is predicting the change in shape of the propagator well. In (b) and (c) the solid line shows the experimental propagator where the flow rate is 10 mL/min. The dashed lines show the simulation predictions of the propagator following polymer treatment. This is done for the two polymer entrapment scenarios considered: polymer adsorption on the solid surface or polymer entrapment in pores where the average velocity was lowest before the polymer was introduced. Clearly the scenario incorporating polymer entrapment in pores provides better agreement with the experimental data.

predictions of the propagators in the original model lattice for observation times of 200 and 500 ms, respectively, and a flow rate of 10 mL/min. The dotted line shows the corresponding experimental results. There is excellent agreement between the simulation and the experimental data. In particular the simulation accurately predicts the change in shape of the propagator as observation time is increased. Note that there are no free parameters in the simulations performed to generate the propagators, and, hence, our model lattice is a good representation of the pore space in the rock core.

In Figure 7b, all propagators correspond to an observation time of 500 ms and a flow rate of 10 mL/min after the polymer treatment, while in Figure 7c all propagators correspond to an observation time of 1,000 ms and a flow rate of 10 mL/min after the polymer treatment. The experimental propagators are shown by the solid lines. The simulation predictions for scenarios (i) and (ii) are shown by the dashed lines. Clearly in both Figure 7b and Figure 7c, scenario (2), where the polymer is retained in comparatively low-velocity pores, provides much better agreement with the experimental result, when compared with scenario (i), where the polymer is absorbed on the solid surface. This was true for all experimental propagators where a significant difference existed between the pretreatment and posttreatment propagators. At short observation times when the experimental pre- and post-treatment propagators were virtually identical, scenarios (i) and (ii) matched the experimental data equally well. Thus, our simulation results agree with our hypothesis that the polymer is predominately retained in low velocity pores.

Conclusions

Displacement propagators were acquired using NMR PFG for a brine solution flowing through a Bentheimer sandstone rock core. This was done both before and after the introduction of a polymer treatment fluid into the pore space. The propagators were seen to change from an exponential shape to a Gaussian shape as the observation time was increased. This transition appeared delayed in the case of the posttreatment propagators. Thus, despite a small decrease in permeability following the polymer treatment (only 25%), a significant change was observed in the shape of the propagators at large values of Δ. A model lattice of the pore space in the rock core was developed and propagators simulated in this lattice. The model pore space had a porosity and a s/v ratio which matched that of the rock core used. The simulated propagators were in good agreement with the experimental propagators, predicting the transition from an exponential shape to a Gaussian shape as observation time was increased. The differences between the pretreatment propagators and the posttreatment propagators were simulated best, by allowing polymer to occupy those pores in which the average velocity of the brine solution was lowest prior to the introduction of the polymer.

Thus, we have verified a novel method of gaining insight into porous material where changes occur in the pore space, using a combination of experiments, using NMR techniques to measure propagators and simulation, based on Lattice–Boltzmann methods, to interpret any changes. This approach is currently being applied to a variety of other porous systems, including deposition from solid suspensions in rock cores and fouling of filters, membranes, and packed-bed reactors.

Notation

A = cross-sectional area of the rock core
d = average displacement in the propagators
D = diffusion coefficient
f = imposed flow rate
g^* = applied magnetic-field gradients
$\boldsymbol{g}$ = strength of applied magnetic-field gradient
$\boldsymbol{P}(\boldsymbol{R},\Delta)$ = displacement propagators
$\boldsymbol{q} = \frac{1}{2}\gamma\delta g$
$\boldsymbol{R}$ = displacement
$\boldsymbol{r}, \boldsymbol{r}'$ = position vectors
RMS = root-mean-squared displacement due to diffusion
s/v = surface-to-volume ratio

Greek letters

δ = duration of magnetic-field gradients
Δ = observation time
ϕ = phase shift of NMR signal
γ = gyromagnetic ratio
σ = porosity

Literature Cited

Akhnoukh, R., J. Leighton, Y. Bigno, E. Quin, G. Catala, L. Silipingo, J. Hemingway, J. Horkowitz, X. Herve, C. Whittaker, K. Kusaka, D. Markel, and A. Martin, "Keeping Producing Wells Healthy," *Oilfield Rev.*, **11**, 30 (1999).

Al-Sharji, H. H., C. A. Gratoni, R. A. Dawe, and R. W. Zimmerman, "Flow of Oil and Water through Elastic Polymer Gels," *Oil Gas Sci. Tech.*, **56**, 145 (2001).

Amin, M. H. G., S. J. Gibbs, R. J. Chorley, K. S. Richards, T. A. Carpenter, and L. D. Hall, "Study of Flow and Hydrodynamic Dispersion in a Porous Medium Using Pulsed-Field-Gradient Magnetic Resonance," *Proc. Roy. Soc. London A*, **453**, 489 (1997).

Baldwin, C. A., A. J. Sederman, M. D. Mantle, P. Alexander, and L. F. Gladden, "Determination and Characterization of the Structure of a Pore Space from 3D Volume Images," *Chem. Eng. Sci.*, **53**, 2117 (1996).

Callaghan, P. T., *Principles of Nuclear Magnetic Resonance Microscopy*, Clarendon Press, Oxford (1991).

Cotts, R. M., J. R. Hoch, T. Sun, and J. T. Markert, "Pulsed Field Gradient Stimulated Echo Methods for Improved NMR Diffusion Measurements in Heterogeneous Systems," *J. Magn. Resonance,* **83**, 252 (1989).

Hurlimann, M. D., K. G. Helmer, L. L. Latour, and C. H. Sotak, "Restricted Diffusion in Sedimentary Rock. Determination of Surface-to-Volume Ratio and Surface Relaxivity," *J. Magn. Resonance Ser. A*, **111**, 169 (1994).

Latour, L. L., P. P. Mitra, R. L. Kleinberg, and C. H. Sotak, "Time-Dependent Diffusion Coefficients of Fluids in Porous Media as a Probe of Surface-to-Volume Ratio," *J. Magn. Resonance, Ser. A*, **101**, 342 (1993).

Lebon, L., L. Oger, J. Leblond, J. P. Hulin, N. S. Martys, and L. M. Schwartz, "Pulsed Gradient NMR Measurements and Numerical Simulation of Flow Velocity Distribution in Sphere Packings," *Phys. Fluids*, **8**, 293 (1996).

Manz, B., P. Alexander, and L. F. Gladden, "Correlations Between Dispersion and Structure in Porous Media Probed by Nuclear Magnetic Resonance," *Phys. Fluids*, **11**, 259 (1999a).

Manz, B., P. B. Warren, and L. F. Gladden, "Flow and Dispersion in Porous Media: A Comparison between Lattice Boltzmann Simulations and Magnetic Resonance Imaging Studies," *AIChE J.*, **45**, 1845 (1999b).

Mitra, P. P., P. N. Sen, L. M. Schwartz, and P. Le Doussal, "Diffusion Propagator as a Probe of the Structure of Porous Media," *Phys. Rev. Lett.*, **68**, 3555 (1992).

Packer, K. J., and J. J. Tessier, "The Characterization of Fluid Transport in a Porous Solid by Pulsed Gradient Stimulated Echo NMR," *Mol. Phys.*, **87**, 267 (1996).
Roberts, J. N., and L. M. Schwartz, "Grain Consolidation and Electrical Conductivity in Porous Media," *Phys. Rev. E.*, **31**, 5990 (1985).
Rothman, D. H., and S. Zaleski, *Lattice-Gas Cellular Automata*, Cambridge Univ. Press, Cambridge (1997).
Sederman, A. J., M. L. Johns, A. S. Bramley, P. Alexander, and L. F. Gladden, "Magnetic Resonance Imaging of Liquid Flow and Pore Structure within Packed Beds," *Chem. Eng. Sci.*, **52**, 2239 (1997).
Seymour, J. D., and P. T. Callaghan, "Generalized Approach to NMR Analysis of Flow and Dispersion in Porous Media," *AIChE J.*, **43**, 2096 (1997).
Stapf, S., K. J. Packer, R. G. Graham, J.-F. Thovert, and P. M. Adler, "Spatial Correlations and Dispersion for Fluid Transport through Packed Glass Beads Studied by Pulsed Field-Gradient NMR," *Phys. Rev. E.*, **58**, 6206 (1998).
Tessier, J. J., and K. J. Packer, "The Characterisation of Multiphase Fluid Transport in a Porous Solid by Pulsed Field Gradient Stimulated Echo Nuclear Magnetic Resonance," *Phys. Fluids*, **10**, 75 (1998).
Van As, H., and D. van Dusschoten, "NMR Methods for Imaging of Transport Processes in Micro-Porous Systems," *Geoderma*, **80**, 389 (1997).

Manuscript received Apr. 16, 2002, and revision received Oct. 8, 2002.